Chemical Engineering Journal 140 (2008) 370–380

Chemical Engineering Journal

www.elsevier.com/locate/cej

# Flow effects on the kinetics of a second-order reaction

Kien T. Nguyen [a], Dimitrios V. Papavassiliou [a,b,*]

[a] *School of Chemical, Biological and Materials Engineering, The University of Oklahoma, 100 East Boyd Street, SEC T-335, Norman, OK 73019 USA*

[b] *Sarkeys Energy Center, The University of Oklahoma, 100 East Boyd, Norman, OK 73019 USA*

Received 9 August 2007; received in revised form 15 October 2007; accepted 17 October 2007

**Abstract**

Flow effects on the kinetics of an isothermal, equimolar, second-order reaction taking place in a channel were investigated using a Lagrangian numerical method. The reactants were released instantaneously from the two opposite walls of the channel into fully developed turbulent or laminar flow. The overall conversion, the residence time and reactor length required to achieve 80% conversion, and the effective reaction rate coefficient were calculated. A correlation of the efficiency ratio, defined as the effective rate coefficient divided by the reaction rate constant, with the flow parameters was found.



*Keywords:* Turbulence; Dispersion; Second-order reaction; Kinetics; Lagrangian simulation methods

## 1. Introduction

Turbulent momentum and scalar transport plays a crucial role in many applications, such as the design of reactors, heat exchangers, and mixing tanks. The investigation of the interactions between chemical reactions, fluid mechanics, and mass transfer in turbulent flows has been limited, at least in numbers of studies, relative to the literature about the velocity field for turbulent flows. The interactions of chemical reactions and transport in tubular reactors have usually been ignored in textbooks and engineering software by assuming a plug flow reactor. In plug flow, the effects of the velocity profile and of the temperature distribution in the direction normal to the vessel walls on the reaction rate are not taken into account. An exception to this trend is the work of Churchill and coworkers, who investigated the interactions of chemical reactions and transport using generalization and asymptotic methods, and developed design equations for tubular reactors, in which the effects of radial variations on the rate of reaction were taken into consideration [1,2].

The inclusion of chemical reactions in a turbulence simulation presents more difficulties than the addition of conservation equations for chemical species [3]. The use of closure models based on the Reynolds analogy is the usual practice in commercial state-of-the-art simulations for chemically reacting flows [3–5]. Sophisticated computational methods, like direct numerical simulation (DNS) methods, have described mainly isotropic turbulence cases in isothermal conditions [6,7]. The coupled reaction-heat-mass transport process has been studied with Eulerian DNS in the case of decaying homogeneous turbulence [8–10]. The focus, however, has been on flames and on generally fast reactions with fixed Schmidt number fluids. Other promising simulations are based on probability density function (PDF) methods [11–14]. Lagrangian PDF methods solve stochastic models (usually the Langevin equation) of the evolution of a probability density function, pdf, for the velocity field in free turbulence. The modeling of pdfs for scalar quantities is more difficult than modeling velocity, and the current models are not completely satisfactory, especially for non-asitropic turbulence (which is the case when a solid wall is present).

In chemical engineering applications, reactions that are slower than combustion and that take place in confined reactors (instead of wall-free turbulence) can be of interest. Based on a Lagrangian numerical methodology (Lagrangian scalar tracking, LST), Mitrovic and Papavassiliou [15] studied the effects of a first order chemical reaction on turbulent mass transfer from

* Corresponding author at: School of Chemical, Biological and Materials Engineering, The University of Oklahoma, 100 East Boyd St., SEC T-335, Norman, OK 73019, USA. Tel.: +1 405 3255811; fax: +1 405 3255813.

*E-mail address:* dvpapava@ou.edu (D.V. Papavassiliou).

1385-8947/$ – see front matter © 2007 Elsevier B.V. All rights reserved.
doi:10.1016/j.cej.2007.10.021

**Nomenclature**

| | |
|---|---|
| A, B | reactants |
| C | product |
| $D$ | diffusivity |
| $Da$ | Damköler number |
| $f$ | collision frequency [collision/(marker × time)] |
| $F_{Ao}$ | initial flow rate of reactant A |
| $h$ | half-height of the channel |
| $k_{A2}$ | reaction rate constant for a second-order reaction |
| $k_{batch}$ | reaction rate constant in a batch reactor |
| $k_{eff}$ | effective reaction rate coefficient |
| $l^*$ | characteristic length scale for wall turbulence, $l^* = \nu/u^*$ |
| npr | number of markers |
| $p$ | probability that a mass marker colliding with another will react |
| $P_1$ | conditional probability for a marker to be at a location $(x, y)$ at time $t$, given that it was released at a known time from a known location in the channel |
| $Pe$ | Péclet number, $Pe = Re \times Sc$ |
| $r_A$ | consumption rate of reactant A |
| $R$ | coefficient of determination for evaluating goodness of fit statistical tests |
| $Re$ | Reynolds number, $Re = u_{max}h/\nu$ |
| $Sc$ | Schmidt number, $Sc = \nu/D$ |
| $t$ | time |
| $t^*$ | characteristic time scale for wall turbulence, $t^* = \nu/(u^*)^2$ |
| $t_o$, $t_f$ | initial and final time of tracking markers ($t_o$ is also the first time step when the first C marker is formed) |
| $t_{1/2}$ | half-life of the second-order reaction |
| $u^*$ | friction velocity, $u^* = (\tau_w/\rho)^{1/2}$ |
| $u_{max}$ | maximum velocity at the center-line of the channel |
| $u$, $v$, $w$ | velocity in the $x$, $y$, and $z$ directions |
| $V$ | reactor volume |
| $X$ | overall reaction conversion |
| $x$, $y$, $z$ | streamwise, normal, and spanwise coordinates |
| $X$, $Y$ | Lagrangian displacement of a marker from the source in the $x$, $y$ directions |

*Greek symbols*

| | |
|---|---|
| $\gamma$ | efficiency ratio |
| $\nu$ | kinematic viscosity |
| $\rho$ | fluid density |
| $\sigma$ | standard deviation of a probability density function |
| $\tau$ | shear stress |
| $\Delta t$ | time step |
| $\Delta x$, $\Delta y$ | bin size in the $x$, $y$ directions |

*Subcripts and superscripts*

| | |
|---|---|
| $\vec{()}$ | vector quantity |
| $()^+$ | value made dimensionless with viscous wall parameters ($u^*$, $t^*$, $l^*$) |
| $()_w$ | value at the wall of the channel |
| $()_o$ | value at initial time |
| $()_\infty$ | value at infinity |
| [] | instantaneous concentration |
| $[]_o$ | initial concentration |

a channel wall to the bulk. In that study, mass markers were released from the wall into a turbulent flow field simulated using DNS and transformed to a product later in time using a Poisson probability function to describe the rate of reaction. Nguyen and Papavassiliou [16] investigated the flow effects on the turbulent mass transfer between a turbulent fluid and the channel wall with the presence of a first-order reaction using the LST methodology. In those numerical experiments, mass markers were released uniformly at the entrance of the channel, diffused from the bulk to the wall and reacted with the wall by a first-order reaction.

In the present study, the effects of flow on the kinetics of an isothermal, elementary, second-order reaction taking place in a channel were investigated using a Lagrangian method. Numerical experiments were conducted, where mass markers of species A and B, representing the reactants, were released instantaneously from two opposite walls of a channel into a fully developed turbulent or laminar flow. The turbulent flow was generated using DNS. The reactants diffused from the wall to the bulk and reacted with each other by a second-order reaction. Since isothermal conditions were assumed, the fluid can be characterized by the Schmidt number, which indicates the relative ease of momentum and mass transport. Although laminar flows are less preferred than turbulent flows in industrial processes, the study of the effects of laminar flows on chemical reactions is also important. Both cases were investigated, and results obtained for both laminar and turbulent flow cases were compared.

## 2. Background

The main objective of this work is to study the effects of laminar and turbulent flows on the kinetics of isothermal second-order reactions, in which particles A and B react to yield C particles

$$A + B \rightarrow C \tag{1}$$

When the initial amount of A and B reactants is equal, the rate equation for this second-order reaction is

$$r_A = -k_{A2}[A]^2 \tag{2}$$

If the reaction takes place in a constant volume batch reactor, the rate law can be written as [17]

$$r_A = \frac{d[A]}{dt} \tag{3}$$

Integrating Eq. (3) from the time when the first C marker is formed, $t_o$, to a time $t$ yields

$$\frac{1}{[A]} - \frac{1}{[A]_o} = k_{A2}(t - t_o) \tag{4}$$

Eq. (4) can be used to calculate the reaction rate constant $k_{A2}$ of a second-order reaction taking place in a constant volume batch reactor. Evaluating Eq. (4) at the reaction half-life yields

$$k_{A2} = \frac{1}{[A]_o t_{1/2}} \tag{5}$$

Eqs. (3)–(5) are only valid for an elementary second-order reaction taking place in a constant volume batch reactor. The differential form of the design Eq. for a plug-flow reactor is [17]

$$\frac{dX}{dV} = -\frac{r_A}{F_{Ao}} \tag{6}$$

In fully developed laminar flows, a parabolic velocity profile is formed and the maximum velocity is at the middle of the channel ($y = 0$), as follows [18]:

$$u = u(y) = u_{max}\left[1 - \left(\frac{y}{h}\right)^2\right] \tag{7}$$

While laminar flows are smooth and orderly, turbulent flows are chaotic. Turbulence is characterized by large scale, observable fluctuations in flow properties. When there is no concentration gradient in the $y$ and $z$ directions and $u$ is constant across the channel, the flow is referred to as a plug flow.

The Damköhler number, $Da$, is a measure of the reaction time scale versus the turbulence time scale, and it is given as follows for a second-order reaction:

$$Da = k_{A2}[A]_o t^* \tag{8}$$

where $k_{A2}$ is the second-order reaction rate constant, which can be calculated using Eq. (4); $[A]_o$ is the concentration at the point of release and can be normalized to one; $t^*$ is the characteristic time scale for wall turbulence [i.e., $t^* = \nu/(u^*)^2$]. The product of $Re$ and $Sc$ is known as the Péclet number, which relates advection rate of a species to its rate of diffusion

$$Pe = Re \cdot Sc \tag{9}$$

## 3. Simulation of a second-order chemical reaction with the Lagrangian scalar tracking method

We call Lagrangian scalar tracking (LST) a methodology that utilizes a tracking algorithm that monitors the space/time trajectories of heat/mass markers in a flow field generated by a computational method, such as DNS. Because of the difficulties in conducting experiments measuring the trajectories of reactants in a turbulent flow field, a computational approach, like LST, can be not only feasible, but also quite insightful for the study of dispersion phenomena.

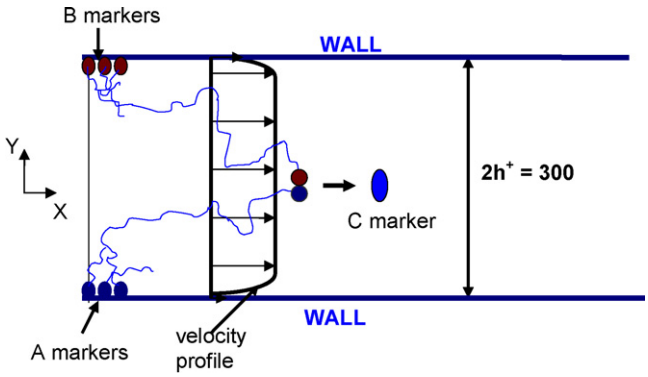


Fig. 1. Schematic of a second-order reaction taking place in a 2D channel with reactants released from two opposite walls.

### 3.1. Turbulent flow and transport simulation

In a turbulent flow field, a mass marker's motion can be decomposed into a convective part and a molecular diffusion part. The convective part can be calculated assuming that the marker velocity is equal to the fluid velocity at the marker position, which is obtained from the DNS velocity field using a high order interpolation scheme [19]. The convective marker displacement is then found as $\Delta\vec{x} = \Delta\vec{u}\Delta t$. The molecular motion after each time step, $\Delta t$, is calculated with a random jump from a Gaussian distribution with zero mean and standard deviation, $\sigma = \sqrt{2\Delta t^+/Sc}$, for each one of the three space dimensions in viscous wall units[1] (this follows from the theory of Brownian motion [20]). For each time step of the flow simulation, therefore, the markers execute two movements, one due to the fluid velocity and one due to the molecular diffusion, as described above. Details about the implementation and validation of the LST methodology, including the stochastic tracking of markers in a turbulent flow field and the statistical post-processing of the results to obtain scalar profiles, can be found in [21–31]. A rather brief description is offered below, with most emphasis on the simulation methodology for second-order reactions. Similar methods for investigating mass transfer have been implemented for flow in porous media [32,33].

A schematic of the problem configuration is shown in Fig. 1. The flow is between two infinite planes and the flow simulation is conducted on a $128 \times 65 \times 128$ grid in $x$, $y$, and $z$ directions for the DNS. The $x$-axis is along the direction of the flow while $y$ is the direction normal to the wall. The half channel height, $h^+$, is 150 in dimensionless viscous wall units. The dimensions of the computational box are $4\pi h \times 2h \times 2\pi h$. The flow is periodic and homogeneous in the $x$ and $z$ directions, with periodicity lengths equal to the dimensions of the computational box in these directions. The fluid is Newtonian, the boundary conditions at the top and the bottom walls are no slip, no penetration, and the Reynolds number, $Re$, based on the mean centerline velocity

[1] In wall turbulence, quantities are usually made dimensionless with the use of the *wall* or *viscous* or *plus* parameters, i.e., the friction velocity, $u^*$, the friction length, $l^*$, and the friction time, $t^*$. Turbulence quantities presented in this work are non-dimensional with the use of these viscous wall scales.

and the half-channel height is 2660, while based on the hydraulic diameter and the bulk velocity is 9040. The DNS used has been validated quite thoroughly in previous work [34,35].

The building block for the Lagrangian formulation is the conditional probability density function $P_1(X - x_o, Y, t - t_o|\overrightarrow{x_o}, t_o)$ for a marker that is released at $\overrightarrow{x_o}$ at time $t_o$ to be at a location $(X, Y)$ at time $t$ (since the flow is homogeneous in the $z$ direction, it is sufficient to examine only the $x$, $y$ functionality of $P_1$). This probability can be interpreted physically as concentration [25,27,36], or as a snapshot of a cloud of contaminants released instantaneously from $x_o = 0$ at $t_o = 0$. This cloud is often called a *puff* of markers.

### 3.2. Laminar flow and transport simulation

The motion of the mass markers in a laminar flow also has a convective part and a molecular diffusive part, like in a turbulent flow. The convective part is obtained using the laminar velocity profile, as given in Eq. (7). The molecular diffusion in a laminar flow is assumed to be of the same nature as in a turbulent flow. No-slip boundary condition was applied. When the $y$ position of a marker in the next time step, $y_{new}$, is greater than 150 (above the upper wall) or less than −150 (below the bottom wall), the marker was assumed to collide with the wall and bounce back from the wall. The bouncing of the markers from the wall follows the law of reflection. The centerline velocity for the laminar flow fields was chosen to be half of the centerline mean velocity for turbulent flow, in order to simulate cases that are physically closer to the laminar flow regime.

### 3.3. Simulation of a reaction in the flow field

In order for marker A and marker B to react with each other, they have to collide. When an A marker and a B marker are within distance $\sigma$ from each other, it was assumed that they collide. The collision frequency, $f$, at a specific time step is defined as the average number of collisions that an A marker has during that time step with B markers. The collision frequency $f$ depends on the fluid, or $Sc$, given isothermal conditions. Not all collisions result in reactions. The reaction probability, $p$, is defined as the number of reactions per collision and has a value from 0 to 1. The algorithm, therefore, checked whether two markers A and B collided at each time step. In order to save computational time, the computational domain was divided into rectangular bins with length $\Delta x^+ = 50$ and height $\Delta y^+ = 10$, which is much larger than $\sigma$. At every time step, each A marker in bin $i$ was checked with all the B markers in bin $i$, and all B markers in the eight bins surrounding bin $i$. If there was a collision, a check was conducted based on the probability $p$ to determine whether a reaction occurred or not. When a reaction occurred, markers A and B were removed from the simulation and a marker of the product C was created. Marker C would follow either the trajectory of the reactant A, or the trajectory of the reactant B, based on a random draw assigning 50% probability to each one of the two possibilities.

A comment is due at this point regarding the choice of the distance between an A and a B marker that is used to determine whether they collide. The collision mechanism between two molecules is a microscopic process that molecular dynamics methods can address. The LST method, however, does not follow individual molecules, and, therefore, a method of estimating $f$ has to be based on a reasonable assumption. The standard deviation of the molecular motion, $\sigma$, was picked, because this is the dominant length scale for the molecular diffusion of the markers in the system. This assumption (that two markers will collide with each other when the distance between them is less than $\sigma$), however, overestimates the frequency of collisions. The overestimation caused by the above assumption is equivalent to choosing a reaction with a higher nominal reaction rate constant, but it can be controlled through the choice of $p$, because the reaction rate constant is also dependent on the value of the reaction probability. In other words, if one had picked a smaller distance than $\sigma$, it would have been equivalent to picking a smaller value of $p$, and if one had picked a larger distance than $\sigma$ it would have been equivalent to picking a larger value of $p$. The value of $p = 1$ has the physical meaning of an instantaneous reaction, and this should be kept in mind when viewing the data appearing in Fig. 9 and on.

In this study, $Sc$ was varied from 0.1 (gas) to 20 (liquid), and $p$ was varied from 0.01 (slow reaction) to 1 (instantaneous reaction). The specific conditions implemented in the simulations are presented in Table 1. The choice of $Sc$ for the laminar flows was made so that their $Pe$ would coincide with the $Pe$ of the turbulent flows. The markers of substance A were released instantaneously at $x = 0$ on the bottom wall, while the same amount of B markers were released instantaneously from the top wall into a fully developed turbulent or laminar flow.

### 3.4. Reaction in a well-mixed batch ractor

This Lagrangian method was also applied to simulate a second-order reaction with isothermal conditions taking place

Table 1
Simulation parameters for the different cases simulated

| | Turbulent flow | Laminar flow | Batch |
|---|---|---|---|
| $Sc$ | 0.1, 0.7, 6, 10 | 0.2, 1.4, 12, 20 | 0.1, 0.2, 0.7, 1.4, 6, 12, 10, 20 |
| $p$ | 0.01, 0.1, 0.25, 0.5, 1.0 | 0.01, 0.1, 0.25, 0.5, 1.0 | 0.01, 0.1, 0.25, 0.5, 1.0 |
| Time step | 0.25 | 1.0 | 1.0 |
| Final time | 3,000 | 15,000 | 15,000 |
| Number of markers A | 145,161 | 145,161 | 145,161 |
| Number of markers B | 145,161 | 145,161 | 145,161 |
| Bin size ($\Delta x$, $\Delta y$) | (50, 10) | (50, 10) | (1, 1) |

in a constant volume, non-agitated, batch reactor. The objectives of simulating a second-order reaction in a batch are to calculate the reaction rate constant, $k$, for different sets of $Sc$ and $p$, and to validate the Lagrangian scalar tracking method described above. At time zero, an equal number of A markers and B markers were distributed randomly in a two-dimensional batch reactor (see Table 1). Isothermal and isotropic conditions were assumed. A simple model of a batch reactor was used, in which the reactor was represented by a 2D square box with dimensions $300 \times 300$. Since there was no flow, the markers only had molecular motions calculated with a random jump from a Gaussian distribution with zero mean and standard deviation, $\sigma = \sqrt{2\Delta t/Sc}$, for each one of the two space dimensions ($x$ and $y$). When an A marker and a B marker were within $\sigma$ from each other, it was assumed that they collided. When the x position or the y position of a marker in the next time step ($x_{new}$ or $y_{new}$) was beyond the boundaries of the batch reactor, it was assumed to collide with the wall and to bounce back from the wall. The bouncing of the markers from the wall followed the law of reflection.

## 4. Results and discussion

### 4.1. Batch reaction simulation

The second-order reaction in a batch reactor was simulated for different sets of $Sc$ and $p$, just like in channel flows. For each ($Sc$, $p$) set, different initial concentrations of A and B were used. For each condition, the instantaneous concentration [A], which is defined as the number of markers per unit area of the 2D batch reactor, was calculated as a function of time. Eq. (4) was used to calculate the nominal reaction rate constant $k$ (or rather $k_{batch}$ for this case) by plotting $1/[A]–1/[A]_o$ against $t$. Fig. 2 shows that the value of $1/[A]–1/[A]_o$ increases linearly with time. The reaction rate constant, which is given by the slope of the lines, does not depend on the initial concentration. This means that the reaction simulated using the LST method behaves like an elementary second-order reaction. Table 2 shows the calculated values of $k$ for different simulation conditions ($Sc$ and $p$). It can be seen that $k$ increases with lower $Sc$ and higher $p$. This is expected, because the markers have larger molecular motion when $Sc$ is lower, hence the probability that a marker will collide with other markers around it is increased. Higher $p$ means more reactions per collision, or a faster reaction.

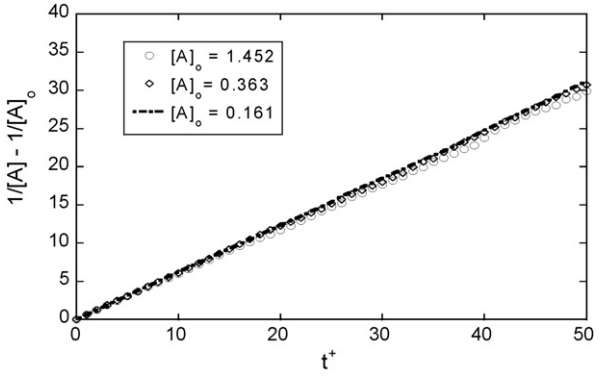


Fig. 2. The calculated value of $1/[A]–1/[A]_o$ for batch reactions as a function of time for different initial concentration values. It is observed that the batch reaction follows the equation of an elementary second-order reaction, and the reaction rate constant does not depend on initial concentration.

Table 2
Reaction rate constant for different simulation condition ($Sc$ and $p$)

| $Sc$ | $p = 0.1$ | $p = 0.25$ | $p = 0.5$ | $p = 1.0$ |
|---|---|---|---|---|
| 0.1 | 4.8606 | 11.9500 | 21.2080 | 28.4720 |
| 0.7 | 0.8194 | 1.7533 | 2.5272 | 4.4537 |
| 6 | 0.0923 | 0.2130 | 0.3576 | 0.5589 |
| 10 | 0.0577 | 0.1332 | 0.2241 | 0.3286 |

Note that applying Eq. (8) and normalizing the initial concentration to be one, the Damköhler number is equal to the reaction rate constant.

### 4.2. Flow and reaction

#### 4.2.1. Effects of the initial number of reactant markers on the reaction kinetics

The number of markers has an important effect on the accuracy of the simulation results. Fig. 3 shows the effects of the number of markers on the overall conversion of the second-order reaction taking place in a turbulent flow channel with an instantaneous release of reactants for $p = 0.01$. The overall conversion is defined as the ratio of the number of A markers at any time divided by the number of A markers originally released into the flow field. It is shown that the overall conversion increases with the number of markers used. The larger the number of markers used, the more accurate the simulations are. However, a larger number of markers also requires more computational time. The

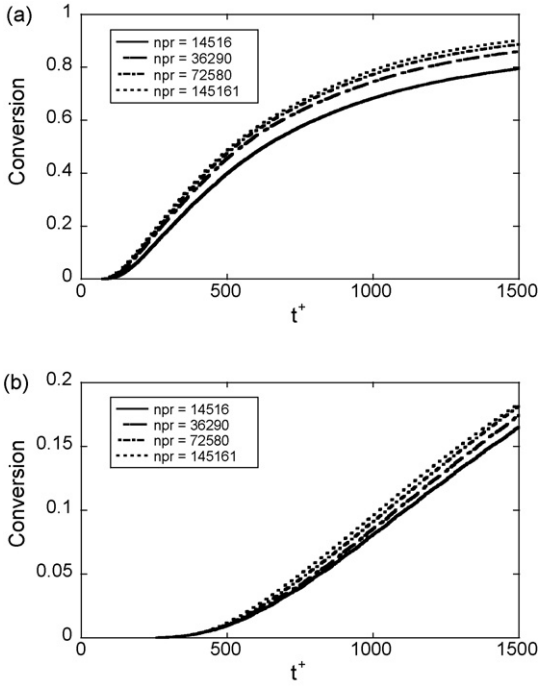


Fig. 3. Effects of the number of reactant markers on the conversion for (a) $Sc = 0.1$ and (b) $Sc = 10$ turbulent flows.

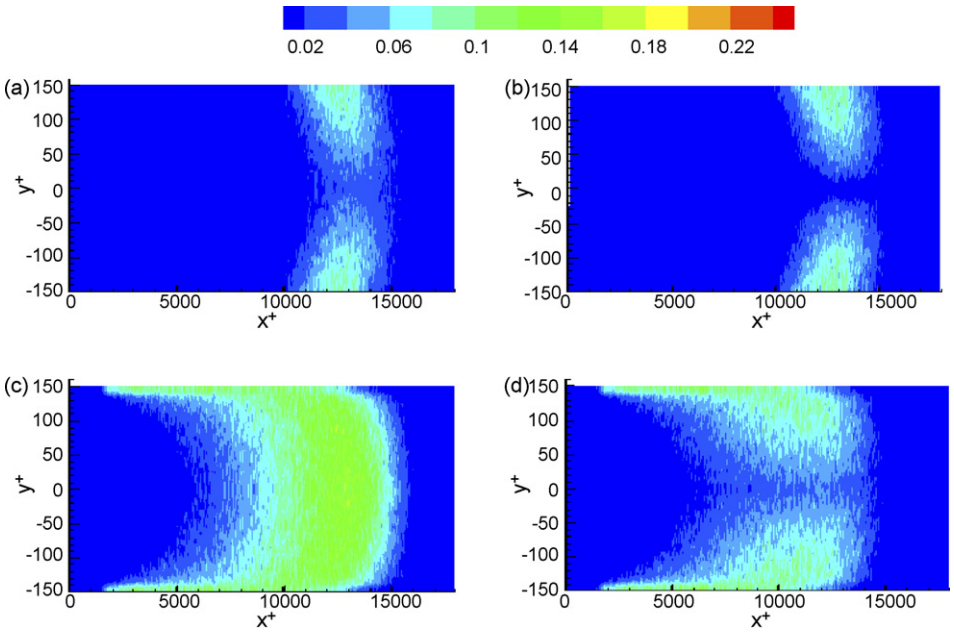


Fig. 4. Mass concentration contours of A and B markers at $t^+ = 1000$ for different reaction rates and different Schmidt number cases: (a) $Sc = 0.1$, $p = 0.01$; (b) $Sc = 0.1$, $p = 0.5$; (c) $Sc = 10$, $p = 0.01$; (d) $Sc = 10$, $p = 0.5$. There is no color differentiation between A and B markers, but note that A markers are released from the bottom wall ($y^+ = -150$), and B markers are released from the top wall ($y^+ = 150$).

increase in the conversion becomes small when the number of markers is larger than 70,000.

### 4.2.2. Concentration profiles

The mass concentration is defined to be the number of markers divided by the area of the computational bin used to calculate Lagrangian statistics and normalized by the concentration at the point of release. The concentration at the point of release equals to the number of released markers (i.e., 145,161) divided by the area of a computational bin, which is a rectangular with $\Delta x^+ = 50$ and $\Delta y^+ = 10$. Using this definition, the mass concentration at the point of release is one at $t^+ = 0$. This is also the maximum concentration throughout the whole channel.

Fig. 4(a–d) shows concentration contours of A and B markers and Fig. 5(a–d) shows concentration contours of C markers for different simulation conditions (different $Sc$ and $p$) for turbulent

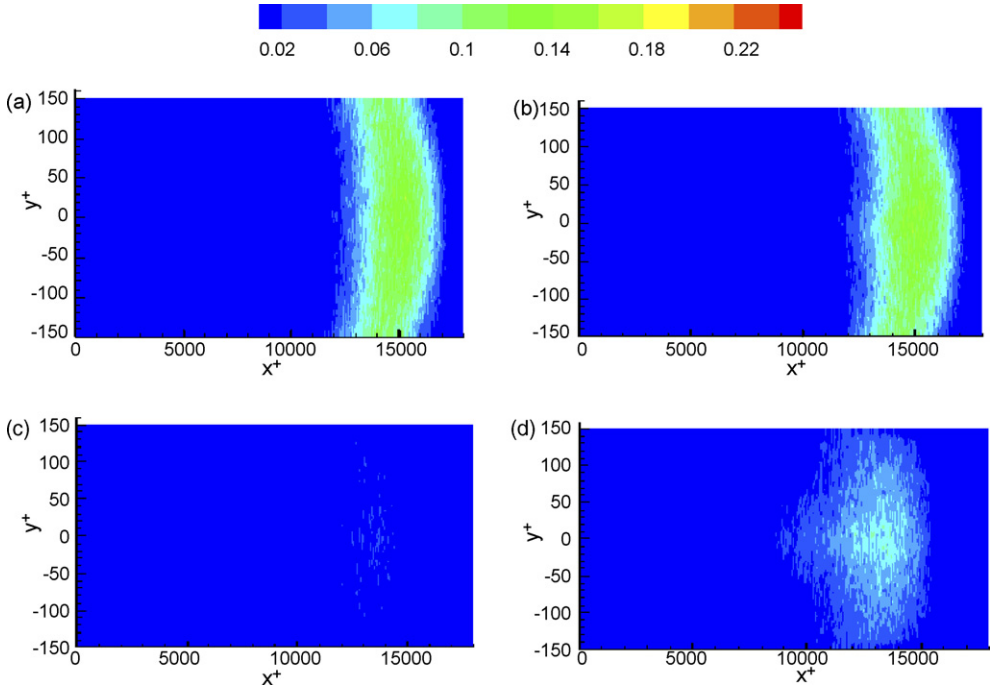


Fig. 5. Mass concentration contours of reaction product C for different reaction rates and different Schmidt number cases at $t^+ = 1000$: (a) $Sc = 0.1$, $p = 0.01$; (b) $Sc = 0.1$, $p = 0.5$; (c) $Sc = 10$, $p = 0.01$; (d) $Sc = 10$, $p = 0.5$.

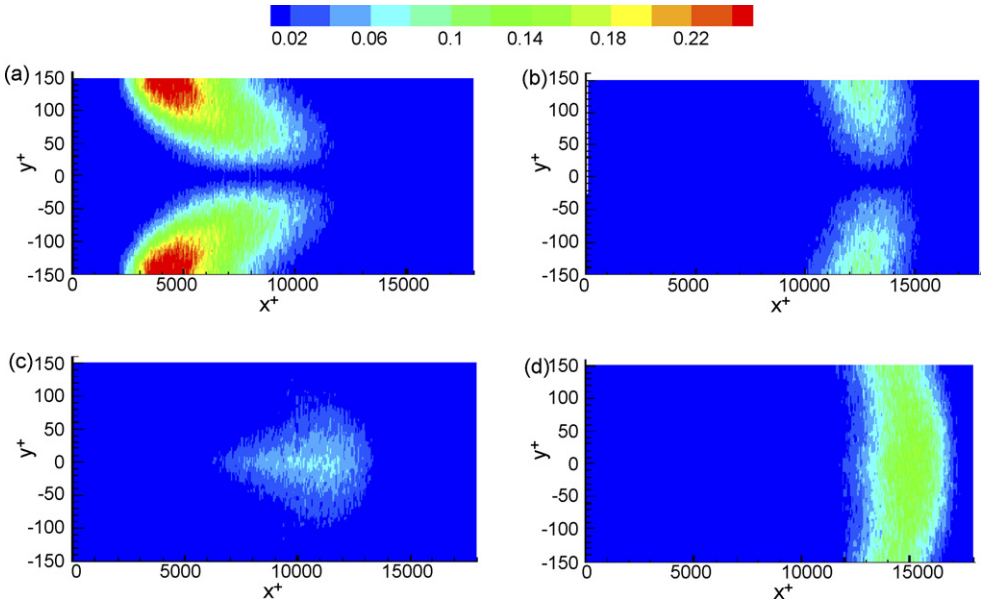


Fig. 6. Mass concentration contours of reactants and products for different flow conditions for $Pe = 266$, $p = 0.5$, $t = 1000$. (a) Reactants A and B in laminar flow; (b) reactants A and B for turbulent flow; (c) product C in laminar flow; (d) product C in turbulent flow. There is no color differentiation between A and B markers, but note that A markers are released from the bottom wall ($y^+ = -150$), and B markers are released from the top wall ($y^+ = 150$).

flows at $t^+ = 1000$. As shown in these figures, both $Sc$ and $p$ have strong effects on the conversion of the second-order reaction. Lower $Sc$ results in faster reactions. At $t^+ = 1000$, approximately 80% of A and B markers have reacted for the cases of $Sc = 0.1$, while most A and B markers have not reacted for the case of $Sc = 10$. This is expected because in a lower $Sc$ turbulent flow, the rate of molecular diffusion is faster and, therefore, it takes less time for A and B markers to diffuse from the location of their source at the walls to the bulk, meet each other, collide and react with each other. Lower $Sc$ also means larger molecular motion and, therefore, a higher probability that a marker collides with other markers around it in one time step. The reaction probability does affect the overall conversion. However, this effect of $p$ is not the same for all $Sc$. For $Sc = 10$, there was a big increase in the number of C markers created when $p$ was increased from 0.01 to 0.5, while no significant change was observed for the case of $Sc = 0.1$ when $p$ was increased from 0.01 to 0.5. For lower $Sc$ fluids, molecular diffusion of the reactants is more prominent and controls the rate of reaction. For higher $Sc$ flows, both the molecular diffusion and the nominal reaction rate (which is proportional to the reaction probability) affect the effective rate of the reaction.

The concentration contours of reactants and products in turbulent flows compared to those in laminar flows for $Pe = 266$ and for $Pe = 26{,}600$ are shown in Figs. 6 and 7, respectively, for different simulation conditions. It can be seen that the second-order reaction taking place in laminar flow is much slower than in turbulent flow. At time $t^+ = 1000$, a very small fraction of A markers has been converted to C markers for the laminar flow at $Pe = 266$ (see Fig. 6(c)), and there is no C formed yet for the laminar flow at $Pe = 26{,}600$ (see Fig. 7(c)). In laminar flow, the fluid flows in smooth layers and there is much less mixing in the direction normal to the walls than in turbulent flows. Therefore, the rate of diffusion of the reactants from the wall to the bulk (which, in laminar flow, occurs due to molecular means) is much slower than the diffusion rate in turbulent flows. In other words, it takes much more time for A and B markers in laminar flow to diffuse towards the center of the channel so that they can react with each other. As a result, the first reaction in laminar flow starts at a much later time than does the first reaction in turbulent flow.

#### 4.2.3. Overall conversion

The overall conversion, $X$, as a function of time is plotted in Fig. 8 for reactions taking place in turbulent flows and laminar flows of different $Pe$ for the case of $p = 0.1$ (Fig. 8(a)) and $p = 0.5$ (Fig. 8(b)). It can be seen that lower $Pe$ flows result in higher overall conversion. Higher $p$ increases $X$ for $Pe \geq 15{,}960$ flows but does not change the overall conversion for smaller $Pe$ flows. Finally, the overall conversion of the second-order reaction in turbulent flows is much higher than in laminar flows, as expected.

Fig. 9(a) shows the number of time steps in wall units to achieve 80% conversion of the reactions taking place in turbulent flows, $t_{80}$, as a function of $Sc$ and $p$. Fig. 9(b) is a plot of the number of time steps in wall units to achieve 10% conversion of the reactions taking place in laminar flows, $t_{10}$, as a function of $Sc$ and $p$. It can be seen that $Sc$ strongly affects the time to achieve 80% overall conversion. As expected the second-order reactions taking place in lower $Sc$ flows are relatively faster. For the case of the turbulent flow with $Sc = 0.1$ and $p = 0.1$, $t_{80}$ is about 990 in wall units. For the case of the turbulent flow with $Sc = 10$ and $p = 0.1$, $t_{80}$ is approximately 3300 in wall units. For laminar flows, $t_{10}$ is 599 for the $Sc = 0.2$, $p = 0.1$ case, and 13,090 for the $Sc = 20$, $p = 0.1$ case. Higher reaction probability, $p$, increases $t_{80}$ for turbulent flows and laminar flows with $Sc \geq 1.4$. However, $p$ does not affect $t_{80}$ for lower $Sc$ flows ($Sc < 1.4$). The overall

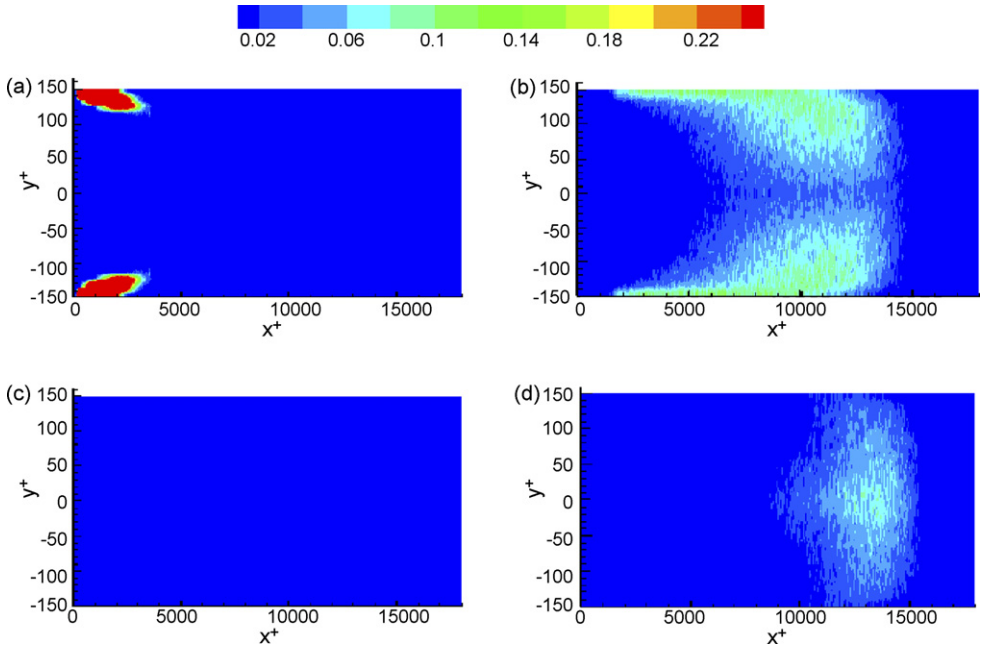


Fig. 7. Mass concentration contours of reactants and products for different flow conditions for $Pe = 26{,}600$, $p = 0.5$, $t = 1000$. (a) Reactants A and B in laminar flow; (b) reactants A and B for turbulent flow; (c) product C in laminar flow; (d) product C in turbulent flow. There is no color differentiation between A and B markers, but note that A markers are released from the bottom wall ($y^+ = -150$), and B markers are released from the top wall ($y^+ = 150$).

rate of the second-order reaction depends on the molecular diffusion, which depends on *Sc*, as well as the reaction probability *p*. However, in smaller *Sc* flows, the molecular diffusion is more prominent and the effects of *p* are diminished. In higher *Sc* flows, in which the rate of molecular diffusion is relatively slower, the effects of both *Sc* and *p* are important. Finally, the reactions taking place in laminar flows were observed to be much slower than those in turbulent flows, as expected.

Fig. 10(a) shows the average *x* positions of all the markers (both reactants and products) at the time when 80% overall conversion is achieved for different turbulent flow and reaction

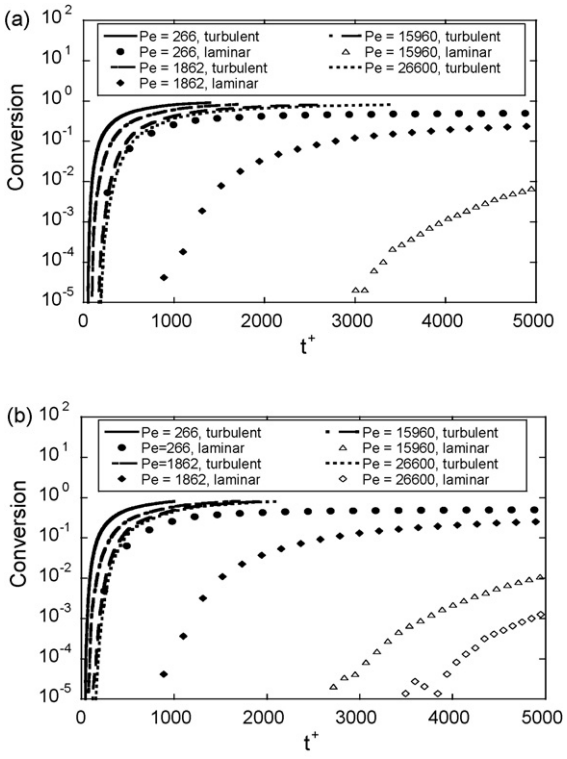


Fig. 8. Overall conversion as a function of time for different flows with (a) $p = 0.1$ and (b) $p = 0.5$.

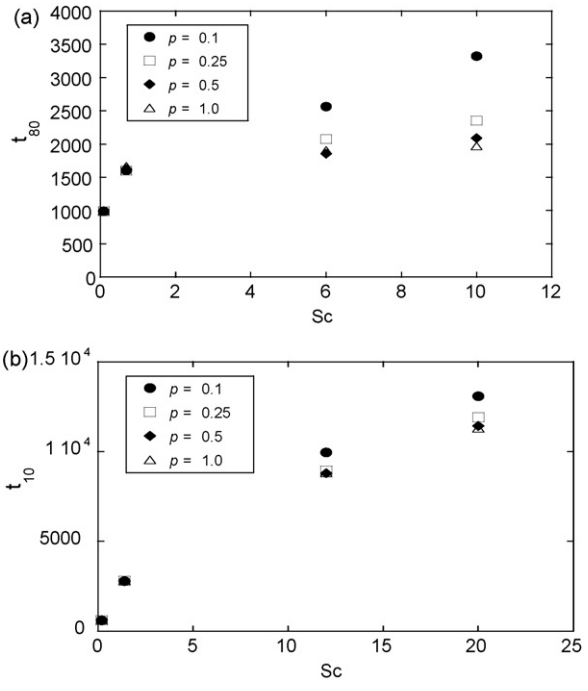


Fig. 9. (a) The time required to achieve 80% overall conversion for reactions taking place in different turbulent flows; (b) time required to achieve 10% conversion for reactions taking place in different laminar flows.

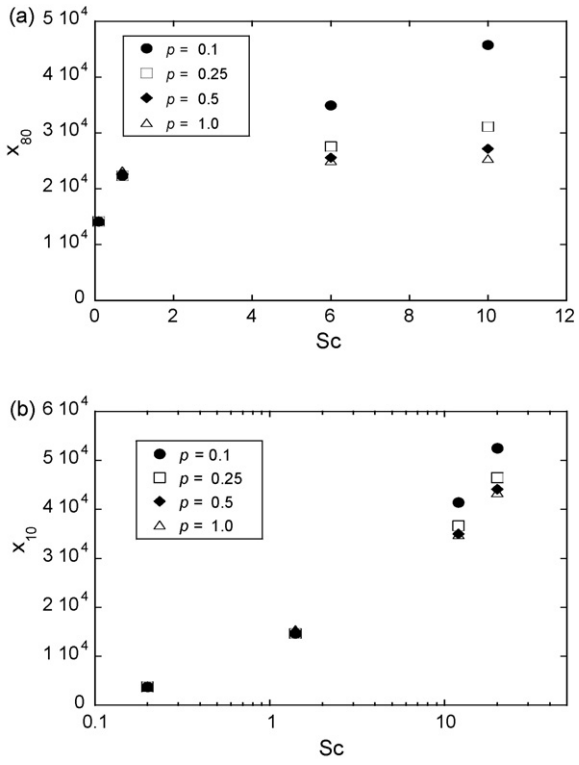


Fig. 10. (a) The reactor length (in wall units) required to achieve 80% overall conversion of the reactions taking place in different turbulent flows; (b) the reactor length required to achieve 10% overall conversion of the reactions taking place in different laminar flows.

conditions (*Sc* and *p*). This average value is called $x_{80}$, which is an approximation of the reactor length required to achieve 80% overall conversion given a set of *Sc* and *p*. Similarly, Fig. 10(b) is a plot of the average *x* positions of all the markers at the time when 10% overall conversion is achieved, or $x_{10}$, for different laminar flow and reaction conditions. Smaller *Sc* flows require shorter reactor length. Higher *p* reduces $x_{80}$ dramatically for the cases of $Sc \geq 6$. However, *p* does not have any effect on $x_{80}$ for lower *Sc* flows. For such flows, it can be seen that the reactor length required for the reaction taking place in laminar flows to achieve 10% conversion is much higher than the length required to achieve 80% conversion in the case of turbulent flow.

#### 4.2.4. Reaction rate constant

The effective reaction rate coefficient, $k_{\text{eff}}$, of a second-order reaction taking place in turbulent flows can be defined as the integral of the product of *f* and *p* from time zero, when the markers are released in the flow field, to the time when 80% of the markers have reacted, as follows:

$$k_{\text{eff}} = \int_{t=0}^{t=t_{80}} f \cdot p \, \mathrm{d}t \tag{10}$$

The above definition is consistent with the collision theory for the interpretation of chemical reactions [37]. Values of $k_{\text{eff}}$ were calculated and plotted as a function of *Sc* and *p*, as shown in Fig. 11. It was found that $k_{\text{eff}}$ increases with smaller *Sc*. In lower *Sc* flows, the reactants can diffuse faster from the walls to the middle of the channel. Therefore, there is less "dead time", in

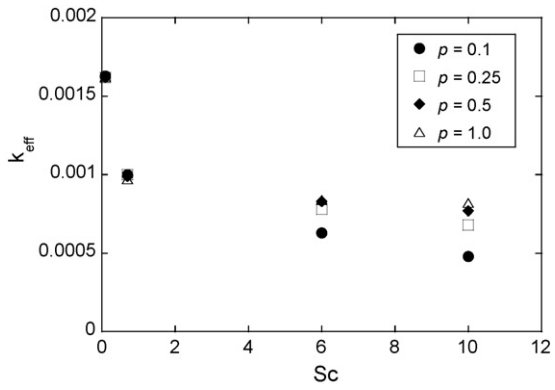


Fig. 11. Effective reaction rate coefficient as a function of *Sc* and *p*.

which no reaction occurs and *f* is equal to zero, in lower *Sc* flows. In addition, smaller *Sc* means larger molecular motions, increasing the probability that an A marker will collide with B markers around it during a time step, thus increasing *f*. Because of these reasons, *f* in lower *Sc* turbulent flows has higher value during the time interval of the integral in Eq. (10). As a result, $k_{\text{eff}}$ is higher in lower *Sc* flows. Higher *p* increases $k_{\text{eff}}$ for turbulent flows with $Sc \geq 1.4$. These *Sc*-dependence and *p*-dependence patterns are consistent with the dependences that *X*, $t_{80}$, $t_{10}$, $x_{80}$, and $x_{10}$ have on *Sc* and *p*. Again, the main factor contributing to this trend is the rate of molecular diffusion, which is a function of *Sc*.

Fig. 12 shows the ratio $k_{\text{eff}}/k_{\text{batch}}$ as a function of *Sc* and *p*. This ratio indicates how fast the reaction takes place in the channel relative to the reaction in a constant volume batch reactor, in which the reactants are premixed before the reaction occurs, given the same type of molecular diffusion (*Sc*) and reaction probability (*p*). This ratio can be called the *efficiency ratio*, $\gamma$. It can be seen that $\gamma$ is very small, ranging from $6 \times 10^{-5}$ to $8 \times 10^{-3}$. This means that the effective reaction rate coefficient is much smaller than the batch reaction rate constant. In a batch, the reactants are assumed to be well-mixed, and the chance that an A marker will find a B marker that is within distance $\sigma$ away from it is much higher. This allows the reaction to occur right at the first time step ($t^+ = 1$). Meanwhile, in a channel, it can take up to thousands of time steps for the A markers and the B markers

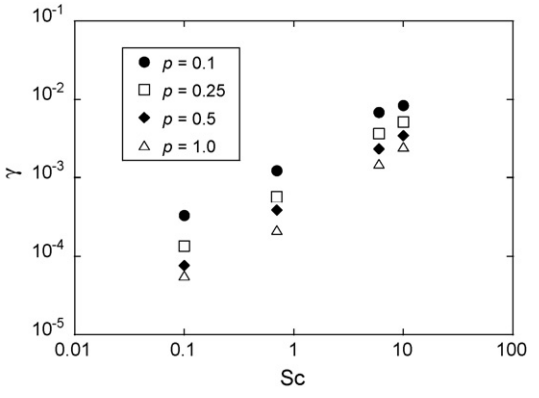


Fig. 12. The efficiency ratio, defined as the effective rate coefficient divided by the reaction rate constant, as a function of *Sc* and *p* for different turbulent flows.

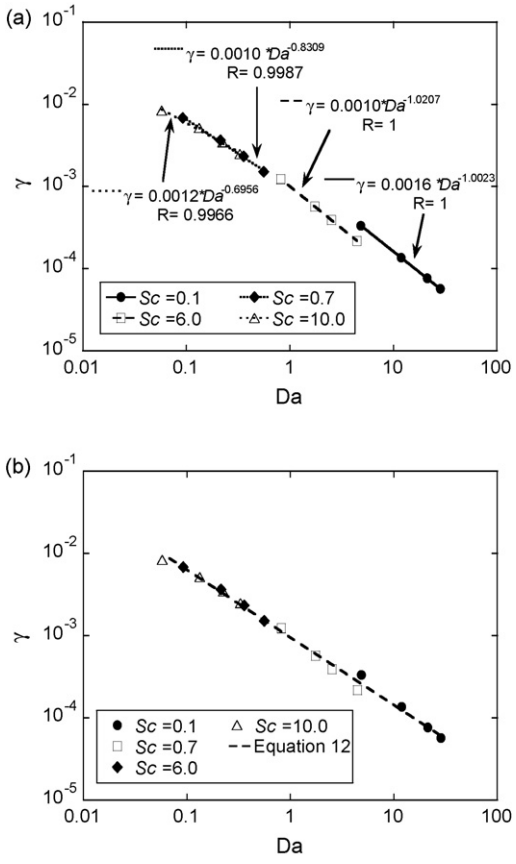


Fig. 13. The efficiency ratio, defined as the effective rate coefficient divided by the reaction rate constant, as a function of: (a) both *Sc* and *Da* for different turbulent flows, and (b) *Da* only for different turbulent flows.

to diffuse from the mass sources located on two opposite walls to the middle of the channel and to mix with each other. The reactants that are closer to the wall will have relatively smaller chance to find reactants of the other kind around them. The efficiency ratio was found to decrease with smaller *Sc* and higher *p*, opposite to the trend observed with $k_{\text{eff}}$, $X$, $t_{80}$, $t_{10}$, $x_{80}$, and $x_{10}$.

In order to obtain a correlation of the efficiency ratio as a function of *Sc* and *Da*, $\gamma$ was plotted versus *Sc* and *Da*, as shown in Fig. 13(a). It can be seen that for each flow condition, meaning for each *Sc*, $\gamma$ follows an exponential function of *Da*. The exponential values are found to be a linear function of *Sc*. The correlation of $k_{\text{eff}}/k_{\text{batch}}$ can then be written as

$$\gamma = \frac{k_{\text{eff}}}{k_{\text{batch}}} = 0.0012 Da^{0.0339Sc-1.0350} \tag{11}$$

If one neglected the *Sc* dependence of the exponential, the correlation of the effective reaction rate with the *Da* would be

$$\gamma = \frac{k_{\text{eff}}}{k_{\text{batch}}} = 0.0010 Da^{-0.8224} \tag{12}$$

with $R^2 = 0.9948$ as shown in Fig. 13(b).

Eqs. (11) and (12) should be used within the *Sc* interval for which they were developed, since very high *Sc* transport is governed by different mechanisms than low *Sc* transport [23]. Even though the exponent of *Da* in Eq. (12) is *Sc* independent, *Da* is a function of diffusivity (due to the dependence of the nominal reaction rate constant on the collision frequency), which in turn is part of the definition of *Sc*.

## 5. Conclusions

The effects of flow on the kinetics of an equimolar second-order reaction taking place in a channel were investigated using a Lagrangian method. The reactants, which are represented by mass markers A and B, were released instantaneously from two different walls of the channel into a fully developed turbulent or laminar flow. Mass markers A and B diffused from the wall sources to the bulk and reacted with each other by an elementary second-order reaction. The reaction was assumed to be isothermal, and the flows were characterized by *Sc*. The Lagrangian method was also used to simulate a second-order reaction in a constant volume batch reactor in order to calculate the reaction rate constant, $k$ or $k_{\text{batch}}$, for each given condition (*Sc* and *p*).

It was found that the calculated reaction rate constant did not depend on the initial concentration. The overall conversion of the second-order reaction taking place in a channel was found to increase with lower *Sc*. Although *p* was found to have no effects on the overall conversion of the reactions taking place in flows with *Sc* less than 1.4, higher *p* increased conversion for flows with $Sc \geq 1.4$. The reactions taking place in lower *Sc* flows were also found to be more efficient because they require less time and shorter reactor length to achieve a high conversion (80%). Higher *p* also increased the efficiency of the reactions taking place in flows with $Sc \geq 1.4$. The effective reaction rate coefficient was calculated and found to increase with lower *Sc* and higher *p*. The efficiency ratio $\gamma$, defined as the effective rate coefficient divided by the reaction rate constant, was found to decrease with lower *Sc* flows and higher *p*. Finally, a correlation of $\gamma$ as a function of *Da* and *Sc* was developed and shown in Eq. (11) and a correlation of $\gamma$ as a function of *Da* only was shown in Eq. (12).

## Acknowledgements

The support of NSF under CBET-0651180 is gratefully acknowledged. This work was also supported by the National Computational Science Alliance under CTS-040023 and by the TeraGrid under TG-CTS070037T, and it utilized the NCSA IBMp690.

## References

[1] S.W. Churchill, Interaction of chemical reactions and transport. 1. An overview, Ind. Eng. Chem. Res. 44 (2005) 5199–5212.
[2] S.W. Churchill, B. Yu, Effects of transport on reactions in homogeneous tubular flow, Ind. Eng. Chem. Res. 45 (25) (2006) 8583–8593.
[3] A.D. Leonard, R.C. Hamlen, R.M. Kerr, J.C. Hill, Evaluation of closure models for turbulent reacting flows, Ind. Eng. Chem. Res. 34 (1995) 3640–3652.
[4] M. Chakrabarti, J.C. Hill, First-order closure theories for serial–parallel reaction in simulated homogeneous turbulence, AICHE J. 43 (4) (1997) 902–911.
[5] Convective heat and mass transfer modeling in the $k$–$\varepsilon$ models, section 11.4.7, in: Fluent 6.2 User's Guide, Fluent Inc., Lebanon, NH, 2007.

[6] A.D. Leonard, J.C. Hill, Direct numerical simulation of turbulent flows with chemical reaction, J. Sci. Comput. 3 (1988) 25–43.
[7] M. Chakrabarti, R.M. Kerr, J.C. Hill, Direct numerical simulation of chemical selectivity in homogeneous turbulence, AIChE J. 41 (1995) 2356–2370.
[8] A.D. Leonard, J.C. Hill, Mixing and chemical reaction in sheared and non-sheared homogeneous turbulence, Fluid Dyn. Res. 10 (1992) 273–297.
[9] O.N. Boratav, S.E. Elghobashi, R. Zhong, On the alignment of strain, vorticity and scalar gradient in turbulent, buoyant, nonpremixed flames, Phys. Fluids 10 (9) (1998) 2260–2267.
[10] W.K. Bushe, R.W. Bilger, Direct numerical simulation of turbulent nonpremixed combustion with realistic chemistry, in: Annual Research Briefs, CTR, Stanford, 1998, pp. 3–22.
[11] S.B. Pope, PDF methods for turbulent reactive flows, Prog. Energy Combust. Sci. 11 (1985) 119–192.
[12] S.B. Pope, Lagrangian PDF methods for turbulent flows, Ann. Rev. Fluid Mech. 26 (1994) 23–63.
[13] P.R. Van Slooten, Jayesh, S.B. Pope, Advances in PDF modeling for inhomogeneous turbulent flows, Phys. Fluids 10 (1) (1998) 246–265.
[14] R.O. Fox, Computational Models for Turbulent Reacting Flows, Cambridge University Press, Cambridge, 2003.
[15] B.M. Mitrovic, D.V. Papavassiliou, Effects of a first-order chemical reaction on turbulent mass transfer, Int. J. Heat Mass Transfer 47 (1) (2004) 43–61.
[16] K.T. Nguyen, D.V. Papavassiliou, Effects of a reacting channel wall on turbulent mass transfer, Int. J. Heat Mass Transfer 51 (2008) 2940–2949.
[17] H.S. Fogler, Elements of Chemical Reaction Engineering, vol. 8, third ed., Prentice Hall, New Jersey, 1999, p. 60.
[18] R.B. Bird, W.E. Stewart, E.N. Lightfoot, Transport Phenomena, vol. 41, second ed., Wiley and Sons, New York, 1960, p. 51.
[19] K. Kontomaris, T.J. Hanratty, J.B. McLaughlin, An algorithm for tracking fluid particles in a spectral simulation of turbulent channel flow, J. Comp. Phys. 103 (1993) 231–242.
[20] A. Einstein, Uber die von der molecular-kinetischen theorie der Warme geforderte Bewegung von in ruhenden Flussigkeiten suspendierten Teacher, Ann. Phys. 17 (1905) 549.
[21] D.V. Papavassiliou, T.J. Hanratty, The use of Lagrangian methods to describe turbulent transport of heat from the wall, Ind. Eng. Chem. Res. 34 (1995) 3359–3367.
[22] D.V. Papavassiliou, T.J. Hanratty, Transport of a passive scalar in a turbulent channel flow, Int. J. Heat Mass Transfer 40 (6) (1997) 1303–1311.
[23] B.M. Mitrovic, P.M. Le, D.V. Papavassiliou, On the Prandtl or Schmidt number dependence of the turbulence heat or mass transfer, Chem. Eng. Sci. 59 (2004) 543–555.
[24] S.S. Ponoth, J.B. McLaughlin, Numerical simulation of mass transfer for bubbles in water, Chem. Eng. Sci. 55 (2000) 1237–1255.
[25] D.V. Papavassiliou, Scalar dispersion from an instantaneous line source at the wall of a turbulent channel for medium and high Prandtl number fluids, Int. J. Heat Fluid Flow 23 (2002) 161–172.
[26] D.V. Papavassiliou, Turbulent transport from continuous sources at the wall of a channel, Int. J. Heat Mass Transfer 45 (17) (2002) 3571–3583.
[27] Y. Mito, J.J. Hanratty, Lagrangian stochastic simulation of turbulent dispersion of heat markers in a channel flow, Int. J. Heat Mass Transfer 46 (6) (2003) 1063–1073.
[28] B.M. Mitrovic, D.V. Papavassiliou, Transport properties for turbulent dispersion from wall sources, AIChE J. 49 (5) (2003) 1095–1108.
[29] P.M. Le, D.V. Papavassiliou, Turbulent dispersion from elevated line sources in plane channel and plane Coquette flow, AIChE J. 51 (9) (2005) 2402–2414.
[30] P.M. Le, D.V. Papavassiliou, On temperature prediction at low Re turbulent flows using the Churchill turbulent heat flux correlation, Int. J. Heat Mass Transfer 49 (2006) 3681–3690.
[31] P.M. Le, D.V. Papavassiliou, Turbulent heat transfer in plane Coquette flow, J. Heat Transfer. Trans. ASME 128 (2006) 53–62.
[32] S.V. Sotirchos, M.M. Tomadakis, A stochastic simulation scheme for studying pore volume trapping in a structure of growing particles, J. Chem. Phys. 109 (11) (1998) 4508–4517.
[33] M.M. Tomadakis, D. Rupani, Diffusion controlled reaction rate, survival probability, and molecular trajectory characteristics in the bulk, transition and Knudsen regime, Chem. Eng. J. 128 (1) (2007) 1–10.
[34] S.L. Lyons, T.J. Hanratty, J.B. McLaughlin, Large-scale computer-simulation of fully-developed turbulent channel flow with heat-transfer, Int. J. Num. Methods Fluids 13 (8) (1991) 999–1028.
[35] A. Gunther, D.V. Papavassiliou, M.D. Warholic, T.J. Hanratty, Turbulent flow in channel at low Reynolds number, Experiments in Fluids 25 (1998) 503–511.
[36] J.E. Cermak, Lagrangian similarity hypothesis applied to diffusion in turbulent shear flow, J. Fluid Mech. 15 (1963) 29–64.
[37] O. Levenspiel, Chemical Reaction Engineering, second ed., John Wiley & Sons Inc., New York, 1972, p. 23.